

Computing the SVD efficiently with photonic chips

Johannes Maly^{*,†}, Korbinian Neuner^{*}, Samarth Vadia^{°,‡*}

^{*} Department of Mathematics, Ludwig-Maximilians-Universität München, Germany

[†] Munich Center for Machine Learning (MCML), Germany

[°] Linque GmbH, Martiusstr. 5, 80802 Munich, Germany

[‡] Institute of Informatics, Ludwig-Maximilians-Universität München, Germany

Abstract

In light of today’s massive data processing, digital computers are reaching fundamental performance limits due to physical limitations and energy consumption. For specific applications, tailored analog systems offer promising alternatives to digital processors. In this work, we investigate the potential of linear photonic chips for accelerating the computation of the singular value decomposition (SVD) of a matrix. The SVD is a key primitive in linear algebra and forms a crucial component of various modern data processing algorithms. Our main insights are twofold: first, hybrid systems of digital controller and photonic chip asymptotically perform on par with large-scale CPU/GPU systems in terms of runtime. Second, such hybrid systems clearly outperform digital systems in terms of energy consumption.

1 Introduction

Since the invention of transistors and integrated circuits around 1950, the processing power of digital computers has been exponentially increasing. This is due to the increasing number of transistors per integrated circuit (Moore’s law) and a downscaling of transistor size (Dennard’s law). Today, fundamental limits in computing performance are being reached as the transistor scaling becomes less effective [27]. Increasing data volume and computational models bring major challenges in the form of massive energy consumption for state-of-the-art computations.

Alternative computing concepts use well-controllable analog systems that occur in nature. The most prominent approach is based on analog electrical circuits where a set of passive and active components can be used to manipulate electric analog signals [18]. Various other physical realizations are also possible, such as molecular computing [4] and fluid computing [23]. An optical analog system is a great physical medium for analog data processing as electromagnetic waves provide multiple degrees of freedom for information encoding and manipulation. Moreover, as the information manipulation in the coherent regime has no heat dissipation, it also provides a potentially orders-of-magnitude improvement in energy efficiency in certain cases.

In this work, we examine how key primitives in linear algebra can be solved efficiently via optical computation on photonic chips. For instance, Reck et al. [21] showed that, for any unitary matrix $\mathbf{U} \in \mathbb{C}^{n \times n}$, there is an experiment, i.e., an assembly of phase-shifters and beamsplitters, which mimics the action of the matrix on n optical channels. This is achieved by decomposing $\mathbf{U} = \mathbf{U}_1 \cdots \mathbf{U}_m$ into a product of unitary matrices $\mathbf{U}_k \in \mathbb{C}^{n \times n}$, each encoding a two dimensional rotation

*Authors are named in alphabetical order, cf. author contribution statement below.

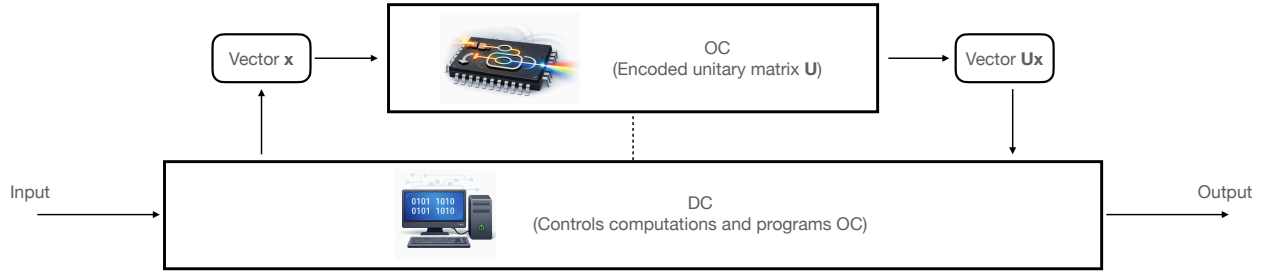


Figure 1: Schematic representation of the hybrid system comprising a digital controller (DC) and an optical chip (OC). Artwork generated using ChatGPT.

embedded into \mathbb{C}^n . The action of \mathbf{U}_k is reproduced by suitably configuring the corresponding phase-shifts in a Mach-Zehnder Interferometer (MZI), and \mathbf{U} can be represented by composing several MZIs. For $\mathbf{z} \in \mathbb{C}^n$ the matrix-vector product $\mathbf{U}\mathbf{z}$ can then be computed with ultra-low latency by encoding the coordinates of \mathbf{z} in the optical channels and passing them through the composition of MZIs. We view such an MZI configuration as a linear programmable optical chip.

By construction, such a chip can encode only *unitary* matrices $\mathbf{U} \in \mathbb{C}^n$. To allow fast matrix-vector products with a general matrix $\mathbf{A} \in \mathbb{C}^{m \times n}$, one could represent \mathbf{A} in terms of its singular value decomposition (SVD) $\mathbf{A} = \mathbf{U}\mathbf{\Sigma}\mathbf{V}^*$. The SVD consists of two unitary transforms $\mathbf{U} \in \mathbb{C}^{m \times m}$, $\mathbf{V} \in \mathbb{C}^{n \times n}$, and a diagonal matrix $\mathbf{\Sigma} \in \mathbb{R}^{m \times n}$ the action of which can be realized by amplification or attenuation of the optical signals.

Since obtaining an SVD of large matrices is costly on digital hardware, this leads to the question whether the SVD of \mathbf{A} can be computed more efficiently by using the optical hardware itself. Efficient analog SVD computation not only entails fast matrix-vector multiplications on such optical chips, but also fast solvers for linear systems since the (pseudo-)inverse of \mathbf{A} can be derived from its SVD as $\mathbf{A}^\dagger = \mathbf{V}\mathbf{\Sigma}^\dagger\mathbf{U}^*$.

1.1 Synopsis of our results

We focus here on computing the SVD of a matrix $\mathbf{A} \in \mathbb{C}^{n \times n}$ by a hybrid system that comprises a digital controller (DC) and an optical chip (OC) realizing unitary vector-matrix products in \mathbb{C}^n . DC can perform digital operations and reprogram the unitary matrix \mathbf{U} encoded on OC, see Figure 1.

The time needed to evaluate $\mathbf{U}\mathbf{z}$ on OC, for some $\mathbf{z} \in \mathbb{C}^n$, is governed by the time needed to encode the entries of \mathbf{z} into n optical channels. It is small compared to the time needed to reprogram the chip to a different unitary matrix \mathbf{U}' , see Table 2. To use this hybrid system effectively for SVD algorithms, one has to well balance the number of matrix re-programmings against the number of matrix-vector products.

We study two algorithms for computing the SVD of a matrix $\mathbf{A} \in \mathbb{C}^{m \times n}$. One naive method which proceeds by iteratively computing QR- and LQ-decompositions of \mathbf{A} in an alternating fashion, and one state-of-the-art method developed by Golub, Reinsch, and Kahan [13, 12] which combines an initial bidiagonalization step with fast chasing of the remaining off-diagonal entries along the diagonal. While the former method is a natural candidate for adaption to the hybrid system by mainly relying on computing orthogonal matrix products, the latter method has been heavily optimized in runtime complexity on digital systems and forms a benchmark for any SVD method.

Our results in Sections 2 and 3 show that, due to slow convergence, neither digital nor hybrid implementation of the naive method can compete with a purely digital, parallelized implementation of the state-of-the-art method. However, we see that by supporting the bidiagonalization step of

Golub-Reinsch-Kahan with OC, the resulting hybrid algorithm reaches an asymptotic runtime on par with its digital counterpart that has access to an unlimited number of GPU cores, while clearly outperforming all digital implementations in terms of expected energy consumption.

1.2 Related work

Before we discuss our results in detail, let us review some of the relevant literature.

SVD algorithms. About 50 years ago, Golub, Reinsch and Kahan [13, 12] proposed an algorithm for computing the singular value decomposition (SVD) of a matrix \mathbf{A} that forms the basis for nearly all modern implementations. The matrix \mathbf{A} is first bidiagonalized via Householder-reflections, followed by a variant of the QR-Algorithm to diagonalize the resulting matrix. The calculation of the singular values alone is reasonably fast, the construction of the unitary matrices \mathbf{U} and \mathbf{V} takes most of the computational effort. We will refer to this algorithm as GRK-SVD in the following.

An alternative and older approach to SVD computation is Jacobi’s method [16], which iteratively applies Givens rotations to \mathbf{A} until it has been diagonalized. While Jacobi’s method is numerically more stable [6], it is slower than GRK-SVD and thus hardly used nowadays. There have been proposed several variations such as the cyclic Jacobi method [10] to accelerate it. Only recently, Drmač and Veselić [6, 7] proposed a sophisticated adaption of Jacobi’s method that preserves its superior numerical stability and can compete with QR-based methods in terms of efficiency.

Architecture of optical chips. The decomposition algorithm one uses to obtain $\mathbf{U}_1, \dots, \mathbf{U}_m$ dictates the required configuration of the MZIs, i.e., the architecture of the optical chip. In the case of Reck et al. [21], $\frac{n(n-1)}{2}$ MZIs have to be arranged in a triangular shape, see Figure 2a, now commonly known as the Reck-architecture.

Building on the work of Reck et al., Clements et al. [3] present an improved rectangular architecture, achieving a higher density of components, see Figure 2b. The number of MZIs needed is still $\frac{n(n-1)}{2}$. However, due to the shorter direct Paths between the different MZI, this architecture is more robust to optical phase mismatch.

Further analog approaches to resource efficient linear algebra. Aifer et al. [1] propose to solve basic tasks from linear algebra such as solving linear systems, inverting matrices, or computing matrix determinants by sampling from the equilibrium state of a suitably initialized thermodynamical system. They provide complexity comparison with state-of-the-art digital solvers of the respective tasks. Their approach is connected to digital Monte-Carlo sampling for solving linear algebra tasks [9].

Huang et al. [15] examine analog accelerators for solving systems of linear equations that are based on ODE simulation. They conclude that such systems can lead to improvements in computation time and efficiency, but also highlight several of their challenges: accurate analog-to-digital conversion, saturation effects for variables with high dynamic range, and scalability of analog systems.

Finally, there has been growing interest in quantum computing architectures based on physical systems utilizing quantum superposition and entanglement. Their main advantage for computation relies on the development of tailored algorithms that can have an exponential speedup in time complexity over classical algorithms [24, 19]. For instance, Harrow et al. proposed a quantum algorithm for solving sparse and well-conditioned n -dimensional linear systems with complexity scaling as $\log(n)$ [14].

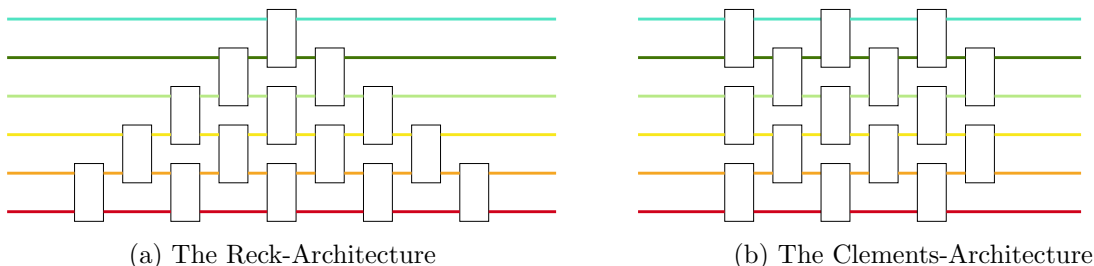


Figure 2: MZI configurations of the optical chip.

However, the latter algorithm comes with massive resource requirements [22] which are critical in light of the difficulties of realizing large-scale quantum hardware [2, 20, 5]. At the moment, the development of new quantum algorithms with proven computational advantage has made little progress. Recent works have even shown that for certain quantum algorithms there are classical algorithms with similar runtime [25, 26].

1.3 Notation

In the following, we denote vectors and matrices in bold lower and upper case letters, i.e., a vector $\mathbf{a} \in \mathbb{R}^d$ can be clearly distinguished from a matrix $\mathbf{A} \in \mathbb{R}^{m \times d}$ with entries \mathbf{A}_{ij} . We abbreviate the identity matrix of dimension k by $I_{k \times k}$. For a vector $\mathbf{z} \in \mathbb{R}^d$ and a matrix $\mathbf{A} \in \mathbb{R}^{m \times d}$, we denote the (Euclidean) ℓ_2 -vector norm of \mathbf{z} by $\|\mathbf{z}\|_2 = (\sum_{i=1}^d z_i^2)^{\frac{1}{2}}$ and the matrix ℓ_2 -norm of \mathbf{A} by $\|\mathbf{A}\| = \sup_{\|\mathbf{z}\|_2=1} \|\mathbf{A}\mathbf{z}\|_2$.

Finally, let us denote the Givens rotation in \mathbb{R}^n of angle θ along the plane spanned by $\mathbf{e}_i, \mathbf{e}_j \in \mathbb{R}^n$, for $i < j$, by $\mathbf{G}_{i,j}^n(\theta) \in \mathbb{R}^{n \times n}$. Whenever clear from context, we will drop the superscript n . The matrix $\mathbf{G}_{i,j}^n(\theta) \in \mathbb{R}^{n \times n}$ differs from the identity matrix in only four positions: when restricted to the i -th and j -th rows and columns $\mathbf{G}_{i,j}^n(\theta)$ is

$$\mathbf{G}_{i,j}^n(\theta) \Big|_{\{i,j\} \times \{i,j\}} = \begin{bmatrix} \cos(\theta) & -\sin(\theta) \\ \sin(\theta) & \cos(\theta) \end{bmatrix},$$

while $[\mathbf{G}_{i,j}^n(\theta)]_{kk} = 1$, for $k \notin \{i, j\}$, and $[\mathbf{G}_{i,j}^n(\theta)]_{kl} = 0$ for any $k, l \notin \{i, j\}$. In our algorithms, we will often characterize θ by its tangent $r = \tan(\theta)$. For brevity, we thus introduce the shorthand notation $\widehat{\mathbf{G}}_{i,j}^n(r) := \mathbf{G}_{i,j}^n(\arctan(r))$ for which

$$\widehat{\mathbf{G}}_{i,j}^n(r) \Big|_{\{i,j\} \times \{i,j\}} = \begin{bmatrix} \cos(\arctan(r)) & -\sin(\arctan(r)) \\ \sin(\arctan(r)) & \cos(\arctan(r)) \end{bmatrix} = \frac{1}{\sqrt{1+r^2}} \begin{bmatrix} 1 & -r \\ r & 1 \end{bmatrix}$$

2 Computing the SVD on the specified hybrid system

Existing routines for computing the SVD of a matrix $\mathbf{A} \in \mathbb{R}^{m \times n}$ have been optimized for digital systems. Given our hybrid system (Figure 1), it is unclear which decomposition algorithm can optimally leverage the fast unitary matrix-vector products of OC.

2.1 SVD via alternating QR decomposition

In a first step, we design a simple method for SVD computation that minimizes the number of DC operations, see Algorithm 1. We will refer to Algorithm 1 as QR-SVD in the following. It

Algorithm 1 : SVDviaQR

Input: $\mathbf{A} \in \mathbb{R}^{m \times n}$

- 1: $\mathbf{U}^{(0)} = \mathbf{I}_{m \times m}$
- 2: $\mathbf{\Sigma}^{(0)} = \mathbf{A}$
- 3: $\mathbf{V}^{(0)} = \mathbf{I}_{n \times n}$
- 4: Initialize $k = 1$
- 5: pick a $\delta > 0$ as the smallest number you want to consider as non-zero
- 6: **while** $\|\mathbf{\Sigma}^{(k)} - \text{diag}(\mathbf{1}) \odot \mathbf{\Sigma}^{(k)}\|_{\infty} > \delta$ **do**
- 7: Decompose $(\mathbf{\Sigma}^{(k)})^{\top} = \tilde{\mathbf{Q}}\tilde{\mathbf{R}}$ via Algorithm 2
- 8: $\mathbf{V}^{(k+1)} = \tilde{\mathbf{Q}}^{\top} \cdot \mathbf{V}^{(k)}$
- 9: $\mathbf{\Sigma}^{(k+\frac{1}{2})} = \tilde{\mathbf{R}}^{\top}$
- 10: Decompose $\mathbf{\Sigma}^{(k+\frac{1}{2})} = \mathbf{Q}\mathbf{R}$ via Algorithm 2
- 11: $\mathbf{U}^{(k)} = \mathbf{U}^{(k-1)} \cdot \mathbf{Q}$
- 12: $\mathbf{\Sigma}^{(k+1)} = \mathbf{R}$
- 13: $k \leftarrow k + 1$
- 14: **end while**

Output: $\mathbf{U} = \mathbf{U}^{(k)}$ (unitary), $\mathbf{V} = (\mathbf{V}^{(k)})^T$ (unitary), and $\mathbf{\Sigma} = \mathbf{\Sigma}^{(k)}$ (approximately diagonal) with $\mathbf{A} \approx \mathbf{U} \cdot \mathbf{\Sigma} \cdot \mathbf{V}^T$

approximates the SVD of \mathbf{A} by alternatingly applying QR- and LQ-decompositions, see Algorithm 2. When implemented on our hybrid system, DC only needs to compute rank-1 matrices to program the required Householder transformations on OC.

While we did not find explicit references for QR-SVD, the method is related to the QR-algorithm for computing the eigenvalues of square matrices [11, 17]. The reason for this lack of references might be that due to the high digital costs of performing even a single QR-decomposition, QR-SVD is impractical on digital systems. Note that if QR-SVD converges, the limit is an SVD of \mathbf{A} .

Lemma 2.1. *Let $\mathbf{A} \in \mathbb{R}^{m \times n}$ be an arbitrary matrix, and let $\mathbf{\Sigma}^{(1)}, \mathbf{\Sigma}^{(\frac{3}{2})}, \mathbf{\Sigma}^{(2)}, \dots$ be the sequence generated by Algorithm 1. If $\mathbf{\Sigma}^{(k/2)}$ converges, then there exists an SVD representation $\mathbf{A} = \mathbf{U}\mathbf{\Sigma}\mathbf{V}^T$ of \mathbf{A} such that for any $\varepsilon > 0$ there exists $k_{\varepsilon} \in \mathbb{N}$ with*

$$\max \left\{ \|\mathbf{U}^{(k/2)} - \mathbf{U}\|_2, \|\mathbf{\Sigma}^{(k/2)} - \mathbf{\Sigma}\|_2, \|\mathbf{V}^{(k/2)} - \mathbf{V}\|_2 \right\} \leq \varepsilon,$$

for all $k \geq k_{\varepsilon}$.

Proof. First note that we have $\mathbf{A} = \mathbf{U}^{(k/2)} \cdot \mathbf{\Sigma}^{(k/2)} \cdot (\mathbf{V}^{(k/2)})^T$ for every k by construction. Assume that $\mathbf{\Sigma}^{(k/2)} \rightarrow \mathbf{\Sigma} \in \mathbb{R}^{m \times n}$. Clearly, there exists $k_{\varepsilon} \in \mathbb{N}$ such that $\|\mathbf{\Sigma}^{(k/2)} - \mathbf{\Sigma}\|_2 \leq \varepsilon$, for all $k \geq k_{\varepsilon}$. Moreover, $\mathbf{\Sigma}$ has to be a diagonal matrix since the iterates $\mathbf{\Sigma}^{(k+\frac{1}{2})}$ are lower triangular while the iterates $\mathbf{\Sigma}^{(k)}$ are upper triangular. Define the set

$$\mathcal{UV}_{\mathbf{\Sigma}} = \{(\mathbf{U}, \mathbf{V}) \in \mathbb{R}^{m \times m} \times \mathbb{R}^{n \times n} : \mathbf{U}, \mathbf{V} \text{ unitary and } \mathbf{A} = \mathbf{U}\mathbf{\Sigma}\mathbf{V}^T\}.$$

Assume that there exists a subsequence $(\mathbf{U}^{(k'/2)}, \mathbf{V}^{(k'/2)})$ such that $\text{dist}((\mathbf{U}^{(k'/2)}, \mathbf{V}^{(k'/2)}), \mathcal{UV}_{\mathbf{\Sigma}}) \geq \varepsilon$, for all k' . Then, there is a convergent subsequence $(\mathbf{U}^{(k''/2)}, \mathbf{V}^{(k''/2)})$ converging to some $(\mathbf{U}, \mathbf{V}) \notin \mathcal{UV}_{\mathbf{\Sigma}}$ such that $\mathbf{U}\mathbf{\Sigma}\mathbf{V}^T = \mathbf{A}$. Contradiction. Hence, we conclude that $\text{dist}((\mathbf{U}^{(k'/2)}, \mathbf{V}^{(k'/2)}), \mathcal{UV}_{\mathbf{\Sigma}}) \rightarrow 0$ which verifies our claim. \square

The performance of QR-SVD on the hybrid system can be optimized by replacing the Householder reflections in Algorithm 2. Indeed, when working with Householder reflections, DC has to compute their decompositions into products of two-dimensional rotations in order to encode them on OC. This decomposition is cubic in the matrix size.

The decomposition step can be bypassed by working with Givens rotations instead. To illustrate this, take \mathbf{a} to be the k -th column of $\mathbf{A}^{(k-1)}$ below the diagonal, i.e.,

$$\mathbf{a} = (\mathbf{A}_{k,k}^{(k-1)}, \mathbf{A}_{k+1,k}^{(k-1)}, \dots, \mathbf{A}_{m,k}^{(k-1)})^\top \in \mathbb{R}^{m-k+1},$$

cf. Algorithm 2. In the k -th iteration, we need to construct a unitary transform that rotates \mathbf{a} to the first unit vector in \mathbb{R}^{m-k+1} . We will do so by replacing the Householder transform with a composition of $m-k$ Givens rotations. Recall the definition of Givens rotations $\mathbf{G}_{i,j}(\theta)$ and $\widehat{\mathbf{G}}_{i,j}(r)$ in Section 1.3.

We first apply a Givens-Rotation $\mathbf{G}_{m-1,m}(\theta_m)$ to \mathbf{a} with θ_m chosen to zero its last entry. This can be computed digitally using a constant number of operations, as only two elements change. Repeating the process, we iteratively construct $\mathbf{G}_{\ell-1,\ell}(\theta_\ell)$, for $\ell = m-1, m-2, \dots, k+1$ to get $\mathbf{G}_{k,k+1}(\theta_{k+1}) \cdots \mathbf{G}_{m-1,m}(\theta_m) \mathbf{a} = \|\mathbf{a}\|_2 \cdot \mathbf{e}_1 \in \mathbb{R}^{m-k+1}$. This costs $\mathcal{O}((m-k)^2)$ digital operations.

Having computed the required rotation angles $\theta_m, \dots, \theta_{k+1}$, we can now encode the respective 2D Givens rotations on the first $m-k$ blocks of the first diagonal of an OC with Reck-architecture, see Figure 2a. Setting all other blocks to identity, OC realizes the unitary transform $\mathbf{G}_{k,k+1}(\theta_{k+1}) \cdots \mathbf{G}_{m-1,m}(\theta_m)$ and can be used to compute $\mathbf{A}^{(k)} = \mathbf{G}_{k,k+1}(\theta_{k+1}) \cdots \mathbf{G}_{m-1,m}(\theta_m) \cdot \mathbf{A}^{(k-1)}$ and $\mathbf{Q}^{(k)} = \mathbf{Q}^{(k-1)} \cdot \mathbf{G}_{m-1,m}^\top(\theta_m) \cdots \mathbf{G}_{k,k+1}^\top(\theta_{k+1})$. To compute $\mathbf{Q}^{(k)}$ with a chip programmed to realize the multiplication with $\mathbf{G}_{k,k+1}(\theta_{k+1}) \cdots \mathbf{G}_{m-1,m}(\theta_m)$, we just pass $(\mathbf{Q}^{(k-1)})^\top$ through the chip and transpose the result. Hence, the chip doesn't need to be reprogrammed for the latter operation.

Our experiments in Section 3 show that QR-SVD on the hybrid system cannot compete with state-of-the-art routines such as GRK-SVD on purely digital systems. The main efficiency bottleneck appears to be the slow convergence of QR-SVD. To reach high-precision solutions, the algorithm requires many iterations.

2.2 Optimizing GRK-SVD for our hybrid system

In light of the unfavorable performance of QR-SVD, we revisit the state-of-the-art algorithm GRK-SVD and examine how it can be optimized for our hybrid system. Let us assume in the following that $\mathbf{A} \in \mathbb{R}^{m \times n}$ with $m \geq n$. GRK-SVD consists of two main components: a bidiagonalization step and a subsequent chasing phase which removes the remaining off-diagonal entries.

In the bidiagonalization step, GRK-SVD applies n Householder-reflections of decreasing size iteratively from each side to reduce \mathbf{A} to bidiagonal shape. The unitary transforms used in the k -th step are

$$\mathbf{U}^{(k)} = \begin{bmatrix} \mathbf{I}_{(k-1) \times (k-1)} & \mathbf{0} \\ \mathbf{0} & \mathbf{U}_{\mathbf{a}-\|\mathbf{a}\|_2 \mathbf{e}_1} \end{bmatrix} \in \mathbb{R}^{m \times m} \quad \text{and} \quad \mathbf{V}^{(k)} = \begin{bmatrix} \mathbf{I}_{(k-1) \times (k-1)} & \mathbf{0} \\ \mathbf{0} & \mathbf{V}_{\mathbf{b}-\|\mathbf{b}\|_2 \mathbf{e}_1} \end{bmatrix} \in \mathbb{R}^{n \times n},$$

where \mathbf{a} and \mathbf{b} are the (partial) k -th column/row of \mathbf{A} that shall be rotated to a unitary vector, and $\mathbf{U}_{\mathbf{z}_U} = \mathbf{I}_{(m-k+1) \times (m-k+1)} - \frac{2}{\|\mathbf{z}_U\|_2^2} \mathbf{z}_U \mathbf{z}_U^\top$ and $\mathbf{V}_{\mathbf{z}_V} = \mathbf{I}_{(n-k+1) \times (n-k+1)} - \frac{2}{\|\mathbf{z}_V\|_2^2} \mathbf{z}_V \mathbf{z}_V^\top$, for $\mathbf{v} \in \mathbb{R}^{m-k+1}$ and $\mathbf{e}_1 \in \mathbb{R}^{m-k+1}$ denoting the first unit vector of the respective dimension. Due to the required matrix-matrix products in each iteration, the bidiagonalization step heavily impacts the computational complexity of GRK-SVD, cf. Table 7.

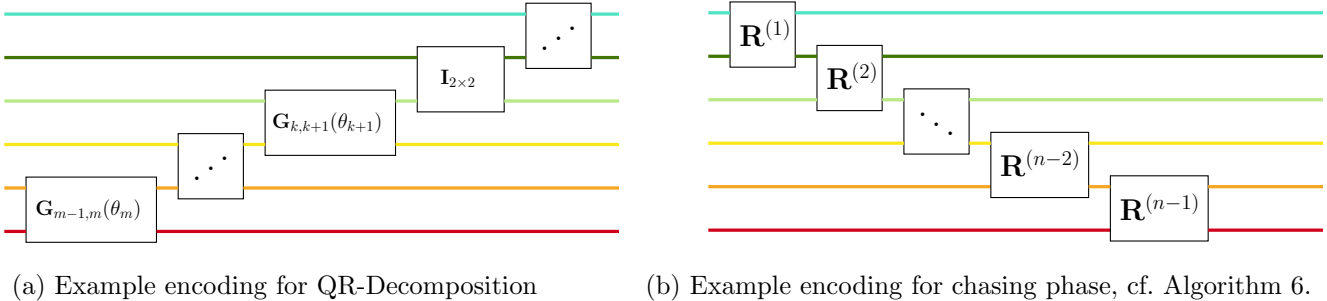


Figure 3: MZI configurations of the optical chip for accelerating (i) the QR-decomposition in QR-SVD and the bidiagonalization step of GRK-SVD, and (ii) the composition of the singular vector matrices in the chasing phase of GRK-SVD. Note that flipping the chip can be done without changing the hardware by reallocating which optical channel corresponds to which coordinate.

At this point, GRK-SVD has constructed a bidiagonal matrix $\mathbf{B} \in \mathbb{R}^{m \times n}$ and unitary matrices $\mathbf{P} \in \mathbb{R}^{m \times m}$, $\mathbf{Q} \in \mathbb{R}^{n \times n}$ such that $\mathbf{A} = \mathbf{PBQ}$. To fully diagonalize \mathbf{B} , GRK-SVD uses Givens rotations and chases the non-zero off-diagonal entries of \mathbf{B} along the second diagonal [13]. By introducing Wilkinson shifts, this diagonalization method exhibits cubic convergence in general, cf. [13]. Due to the bidiagonal shape of \mathbf{B} , each multiplication with a Givens rotation can be computed quickly, even on a digital system. Combined with the cubic convergence, this leads to low computational complexity of the chasing step, see Table 7.

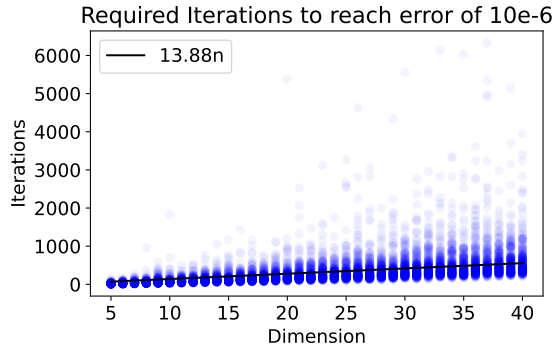
When optimizing GRK-SVD for our hybrid system, only the bidiagonalization step needs to be changed substantially.¹ Since this proceeds by interleaving the iterations of a QR- and an LQ-decomposition, we can slightly modify the scheme for accelerating the QR-decomposition of QR-SVD described in Section 2.1, see Algorithm 6. The impact on computational complexity is illustrated in Table 9.

3 Experiments

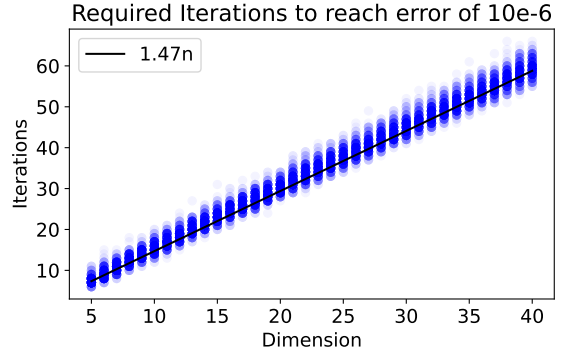
We will now present evidence for our main claims that (i) even a hybrid implementation of QR-SVD cannot compete with digital GRK-SVD, and that (ii) a hybrid implementation of GRK-SVD shows clear benefits when compared to its digital counterpart, both in terms of runtime and energy consumption.

To evaluate the effective runtime, we first subdivide both algorithms into basic operations and count the number of each operation. We consider three different versions of each algorithm: a purely digital implementation with sequential computing (**Digital-SingleCore**), a purely digital

¹Indeed, applying Givens rotations to a bidiagonal matrix is of complexity $\mathcal{O}(1)$ such that using OC in the chasing phase would bring no relevant performance gain when computing the singular values. The only change in the hybrid implementation of the chasing phase is to directly build the two unitary transformation matrices containing the singular vectors on OC. Instead of computing them as a product of several Givens rotations, one can encode the single Givens rotations in 2×2 -blocks of OC. Figure 3b shows the exact arrangement of Givens-matrices on OC, separately for the two steps of our algorithm.

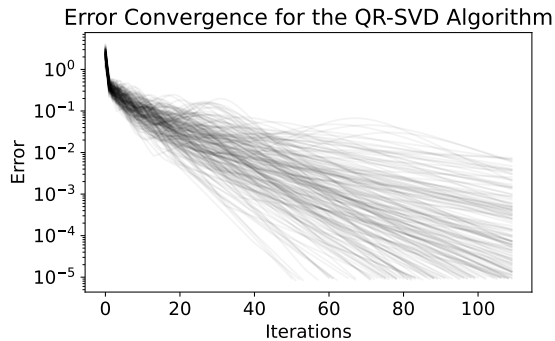


(a) QR-SVD

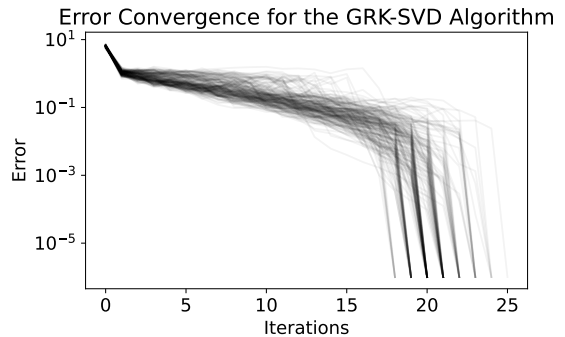


(b) GRK-SVD

Figure 4: Number of iterations to reach target precision of 10^{-6} for QR-SVD and GRK-SVD. Linear best fit for medians is $y = mx + b$, with $m \approx 13.88$ and $b \approx -78.61$ (QR-SVD) and $m \approx 1.47$ and $b \approx 0.83$ (GRK-SVD).



(a) QR-SVD



(b) GRK-SVD

Figure 5: Error on off-diagonal entries of $\Sigma^{(k)}$ when applying QR-SVD and GRK-SVD to 200 randomly drawn matrices in $\mathbb{R}^{15 \times 15}$.

implementation in which matrix operations are executed on GPUs with an unlimited number of cores (**Digital-MultiCore**), and a hybrid implementation in which parts of the operations are executed on the photonic chip (**Hybrid**). The resulting operation counts for QR-SVD and GRK-SVD are summarized in Tables 5–6 and Tables 7–9, respectively. Further details on how these counts have been derived are discussed in Appendix A.

We then fix a target precision of 10^{-6} for the off-diagonal entries of $\Sigma^{(k)}$ and estimate the expected number of iterations for each algorithm, by linear regression over random executions. Figure 4 shows that the expected number of iterations can be well-described by a linear fit. Note, however, that QR-SVD requires more iterations in general and shows a large variance of the necessary number of iterations. The worse convergence rate of QR-SVD is illustrated in Figure 5.

By combining the expected number of iterations of both algorithms in Figure 4 with the counts of computational operations per method in Tables 5–9 and multiplying them with time estimates for single CPU/GPU/photonic chip operations, see Tables 1 and 2, we obtain runtime estimates for all described methods. The code to reproduce the presented experiments is provided at <https://github.com/Korbinian-Neuner/Computing-the-SVD-with-Photonic-Chips/tree/main>.

Operation	relative time required
Addition	1
Multiplication	1
Division	20
Square root	15
Addition (GPU)	4
Multiplication (GPU)	4
Chip Configuration	10000
Chip Operation	50

Table 1: Relative time cost estimates for different operations on our model systems [28]. Estimates for DC were made by assuming a 4GHz CPU and a GPU of around 1GHz (0.25 ns represent one time unit here), cf. Table 2. We infer from the Agner-Fog instruction tables [8] that the time costs for divisions are a bit more than for the square root.

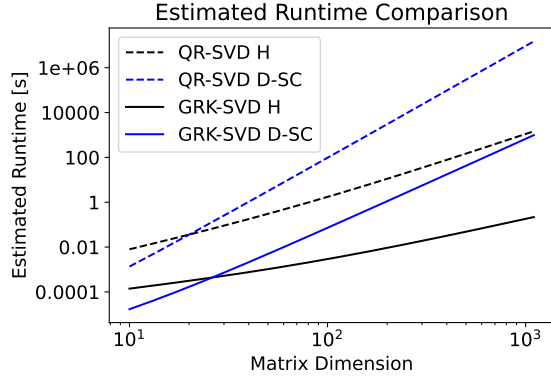
Operation	time (fastest)	time (average)
Chip Configuration	1 ns	1 ms
Chip Operation	10 ps	1 ns
Light traveling time	1 ns	10ns

Table 2: Absolute time cost estimates for different operations on an optical chip (estimates provided by Linque). Note that the light traveling time through the chip only affects latency, not throughput. Nevertheless, for the sake of comparison we take very conservative estimates of 2.5 ms for chip configuration and 12.5 ns for chip operation

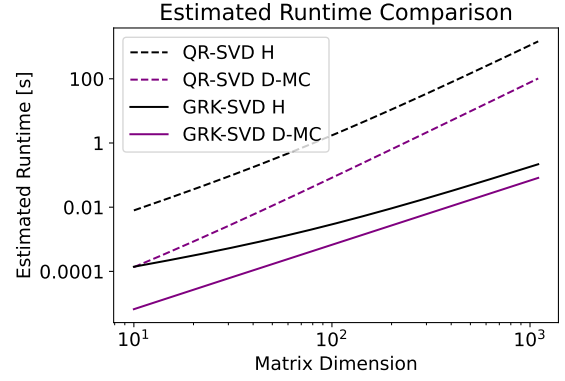
Experiment 1 — Runtime. In the first experiment, we compare the expected runtime of QR-SVD and GRK-SVD in all types of implementation, i.e., digital single-core, digital multi-core, and hybrid (D-SC,D-MC,H). For simplicity, we only consider the SVD of square-matrices, i.e., $m = n$. Figure 6 shows that the hybrid implementation of QR-SVD is clearly outperformed by the digital implementations of GRK-SVD. This is as expected considering the slower convergence rate of QR-SVD. At the same time, we see that the hybrid implementation of GRK-SVD asymptotically outperforms the D-SC implementation of GRK-SVD, and performs on par with the D-MC implementation using an unlimited number of GPU cores.

Experiment 2 — Energy consumption. In the second experiment, we compare the expected energy consumption of QR-SVD and GRK-SVD in all types of implementation, i.e., digital single-core, digital multi-core, and hybrid (D-SC,D-MC,H). Again, we only consider the SVD of square-matrices. The energy consumption of the CPU is calculated by multiplying the number of operations executed on the CPU by the average energy cost per FLOP. This means that we treat the energy costs of different types of operations to be the same. We proceed analogously for the GPU where we use the counts of actual GPU operations, see Table 3. The latter are computed as the difference between the total number of operations and the parallelized count of the corresponding operation. In case of the hybrid implementation, we add the expected energy consumption of the OC operations, see Table 4 to the expected energy consumption of the CPU operations. Figure 7 illustrates that the hybrid implementation of GRK-SVD asymptotically outperforms all digital implementations.

On the validity of our comparison. Figure 8 illustrates that our predicted runtimes match

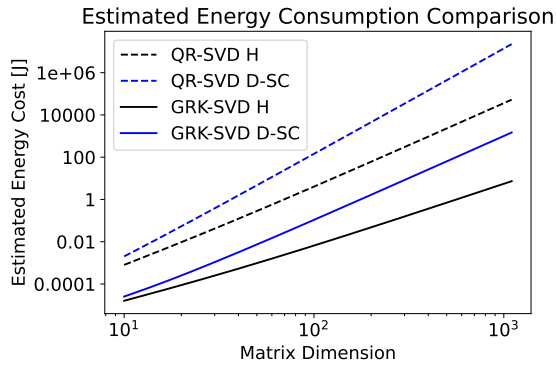


(a) D-SC vs H

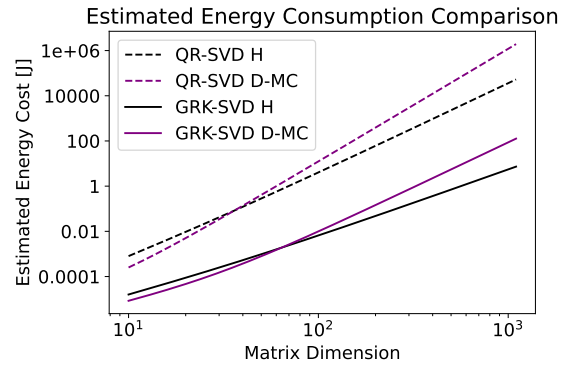


(b) D-MC vs H

Figure 6: Comparison of expected runtime of QR-SVD (D-SC,D-MC,H) and GRK-SVD (D-SC,D-MC,H).



(a) D-SC vs H



(b) D-MC vs H

Figure 7: Comparison of expected energy consumption of QR-SVD (D-SC,D-MC,H) and GRK-SVD (D-SC,D-MC,H).

Processor	energy cost per bit	total cost
CPU (per time unit)	5.86 pJ	375 pJ
GPU (per FLOP)	0.5 pJ	32.24 pJ

Table 3: Absolute energy cost estimates for one time unit on CPU and GPU. The values are based on an AMD Ryzen 7 9800x3d consuming on average around 120W on 8 cores, which at 4GHz corresponds to 375 pJ per cycle per core, and an NVIDIA B200 consuming at peak around 1200W while reaching $37.22 * 10^{12}$ double flops, which amounts to around 32.24 pJ per operation, or 0.5 pJ per FLOP and bit. These specifications can be found on the webpages of AMD and NVIDIA.

Operation	energy cost per bit	total cost
Chip Configuration	20 pJ	$640n(n - 1)$ pJ
Chip Operation	5 pJ	$320n$ pJ

Table 4: Absolute energy cost estimates for different operations on an optical chip (estimates provided by Linque). The total cost is obtained by taking double precision (64bit) and a chip size of n .

the actual runtime of QR-SVD and GRK-SVD. In the case of GRK-SVD a factor 6 has to be multiplied. This can be explained by the missing count of memory operations which affect GRK-SVD more heavily than QR-SVD. Since the ignored memory costs have a higher impact on purely digital implementations, this does not weaken our claim that the hybrid implementation is competitive even under conservative time estimates.

Finally, note that the implementations of QR-SVD and GRK-SVD in Algorithms 1 and 4 are stated in a way to enhance conceptual clarity, not to optimize their actual runtime. Nevertheless, Figure 9 shows that, as the matrix dimension grows, our predicted runtimes are a clear lower bound on the actual runtimes of optimized LAPACK routines. As before, this discrepancy can be explained by the ignored memory costs. We reiterate that our runtime and energy consumption comparisons are thus strongly favoring the digital implementations which require more memory operations in general.

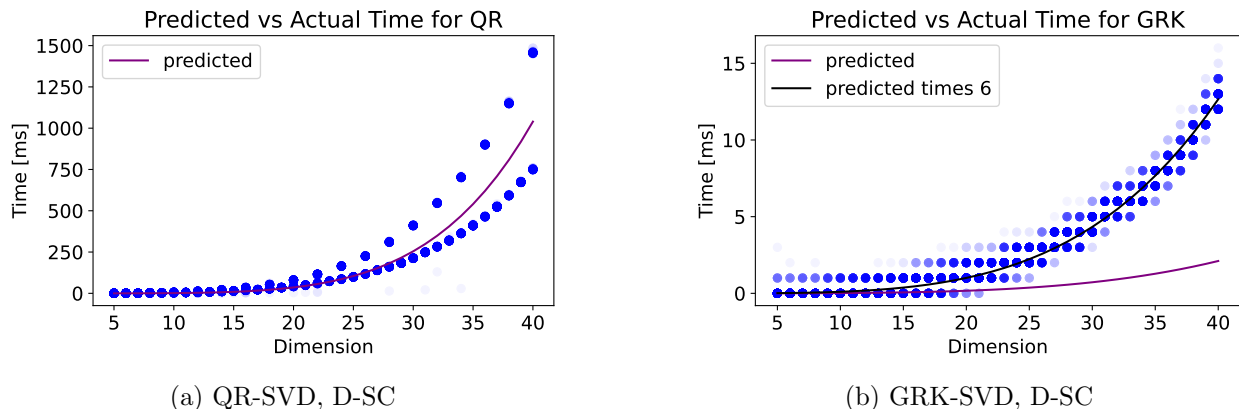
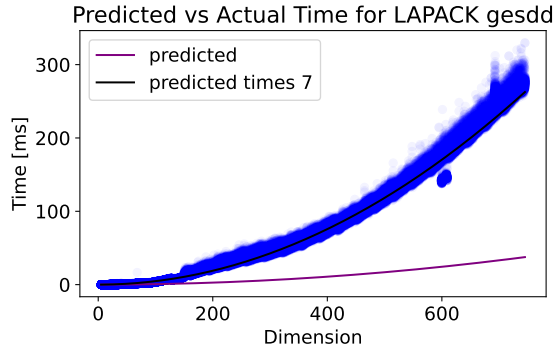
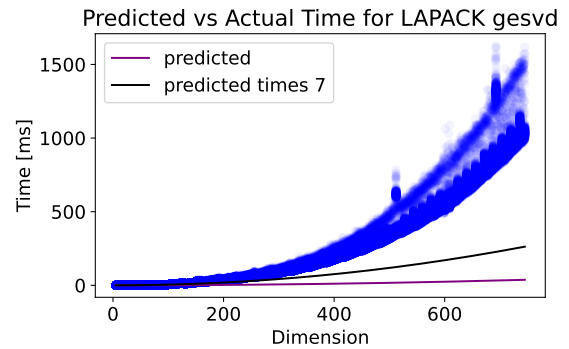


Figure 8: Experimental verification of our time cost model comparing estimated and actual runtime of our digital implementations of QR-SVD and GRK-SVD.



(a) GRK-SVD D-MC vs LAPACK gesdd



(b) GRK-SVD D-MC vs LAPACK gesvd

Figure 9: Experimental verification of our time cost model against the optimized LAPACK routines gesdd and gesvd. Here we used the runtime estimates for the D-MC implementation.

4 Discussion

The presented analysis shows that photonic chips yield promising solutions for increasing the energy efficiency of purely digital systems. Computing the SVD is a core component of various modern data processing algorithms. Efficiency gains thus carry over to a multitude of methods including other linear algebraic primitives such as matrix inversion and solving linear systems. In future work it would be desirable to identify further basic operations that can be outsourced to photonic components, and to design advanced hybrid methods for SVD computations and other important primitives, challenging digital state-of-the-art algorithms both in terms of runtime and energy efficiency.

Author contribution statement

JM and SV initiated the conducted research by joint discussions. JM carried out the main conceptual work and wrote great parts of the manuscript. KN optimized the hybrid implementations of the methods, carried out the operation counts, the experiments, and the computations of energy consumption, and provided detailed pseudocode of all involved methods. SV provided specifications of the discussed optical chips. KN and SV helped finalizing the manuscript.

Data and code availability statement

All code to reproduce the experiments presented here can be accessed via <https://github.com/Korbinian-Neuner/Computing-the-SVD-with-Photonic-Chips/tree/main>. The datasets generated and/or analyzed during the current study are available here: <https://github.com/Korbinian-Neuner/Computing-the-SVD-with-Photonic-Chips/tree/main/Data>.

A Operation counts of algorithms

We present here Tables 5–9. When counting the number of operations, we used the following conventions.

Operation	Count (total)	Count (parallelized)	actual GPU count
Addition	$(m^3n + m^3 + 2m^2n - \frac{1}{3}mn^3 + \frac{19}{3}mn - m + \frac{2}{3}n^4 + \frac{5}{3}n^3 + \frac{1}{3}n^2 + \frac{19}{3}n - 7)C$	$(3mn + 5n - 4)C$	$(m^3n + m^3 + 2m^2n - \frac{1}{3}mn^3 + \frac{10}{3}mn - m + \frac{2}{3}n^4 + \frac{5}{3}n^3 + \frac{1}{3}n^2 + \frac{4}{3}n - 3)C$
Addition (GPU)	-	$(2mn + m + 9n - 5)C$	-
Multiplication	$(m^3n + m^3 + 3m^2n - \frac{1}{3}mn^3 - mn^2 + \frac{16}{3}mn - m + \frac{2}{3}n^4 + \frac{7}{3}n^3 + \frac{1}{3}n^2 + \frac{8}{3}n - 5)C$	$(3mn + 3n - 3)C$	$(m^3n + m^3 + 3m^2n - \frac{1}{3}mn^3 - mn^2 + \frac{7}{3}mn - m + \frac{2}{3}n^4 + \frac{7}{3}n^3 + \frac{1}{3}n^2 - \frac{1}{3}n - 2)C$
Multiplication (GPU)	-	$(2mn + m + 7n - 4)C$	-
Division	$(2n - 1)C$	$(2n - 1)C$	-
Square root	$(4n - 2)C$	$(4n - 2)C$	-

Table 5: Operation counts for QR-SVD. Total count corresponds to QR-SVD (D-SC), parallelized count corresponds to QR-SVD (D-MC). The actual GPU count shows how many of the corresponding operation are actually performed on the GPU in the D-MC implementation, which is relevant when estimating the energy consumption.

Operation	Count
Addition	$(5mn - 5n)C$
Multiplication	$(4mn - 4n)C$
Division	$(3mn - 3n)C$
Square root	$(2mn - 2n)C$
Chip configuration	$(m + n)C$
Chip operation	$(m^2 + 2mn + n^2)C$

Table 6: Operation counts for QR-SVD (H).

We count subtraction and multiplication by -1 as single additions. We do not count operations to calculate indices and storage related operations since these are hard to track explicitly. While the time costs for memory calls are relevant for all implementations, omitting them is favorable for the digital implementations since OC does not require memory operations. We do not parallelize the multiplication of a bidiagonal matrix with a Givens rotation in the hybrid system since it only requires 4–6 operations of the digital controller.

Due to the travelling time of light there is a small dependence of the time estimates in Table 2 on the size of the photonic chip. We implicitly fixed the chip length in our time estimates.

Finally, we assume that the digital system uses a single-core CPU and a GPU with potentially infinitely many cores, i.e., one GPU operation corresponds to an arbitrary number of elementary operations that are fully parallelizable.

B Pseudocode for all presented algorithms

We present here the detailed pseudocode for all algorithms discussed in Sections 2 and 3:

- The basic QR-decomposition (Algorithm 2)
- The GRK-SVD bidiagonalization step (Algorithm 3)

Operation	Count in Bidiag	Count in QR-Iter
Addition	$m^3n + 2m^2n - \frac{1}{3}mn^3 - mn^2 + \frac{19}{3}mn - m + \frac{2}{3}n^4 - \frac{1}{3}n^3 - \frac{2}{3}n^2 + \frac{4}{3}n - 8$	$(2n - 2)mC + (2n^2 + 17n - 16)C$
Multiplication	$m^3n + 3m^2n - \frac{1}{3}mn^3 - 2mn^2 + \frac{16}{3}mn - m + \frac{2}{3}n^4 + \frac{1}{3}n^3 - \frac{5}{3}n^2 - \frac{1}{3}n - 5$	$(4n - 4)mC + (4n^2 + 24n - 27)C$
Division	$2n - 2$	$(4n - 3)C$
Square root	$4n - 4$	$(2n - 1)C$

Table 7: Operation counts for GRK-SVD (D-SC).

Operation	Count in Bidiag	Count in QR-Iter
Addition	$3mn + 2n - 5$	$7nC$
Addition (GPU)	$2mn + 6n - 8$	$(4n - 4)C$
Multiplication	$3nm - 3$	$(4n + 5)C$
Multiplication (GPU)	$2mn + 4n - 6$	$(8n - 8)C$
Division	$2n - 2$	$(4n - 3)C$
Square root	$4n - 4$	$(2n - 1)C$

Table 8: Operation counts for GRK-SVD (D-MC).

- The full GRK-SVD algorithm (Algorithm 4)
- The QR-decomposition optimized for the hybrid system (Algorithm 5)
- The GRK-SVD bidiagonalization step optimized for the hybrid system (Algorithm 6)
- The full GRK-SVD algorithm optimized for the hybrid system (Algorithm 7)

References

- [1] Maxwell Aifer, Kaelan Donatella, Max Hunter Gordon, Samuel Duffield, Thomas Ahle, Daniel Simpson, Gavin Crooks, and Patrick J Coles. Thermodynamic linear algebra. *npj Unconventional Computing*, 1(1):13, 2024.
- [2] Rupak Biswas, Zhang Jiang, Kostya Kechezhi, Sergey Knysh, Salvatore Mandra, Bryan O’Gorman, Alejandro Perdomo-Ortiz, Andre Petukhov, John Realpe-Gómez, Eleanor Rieffel, et al. A nasa perspective on quantum computing: Opportunities and challenges. *Parallel Computing*, 64:81–98, 2017.
- [3] William R. Clements, Peter C. Humphreys, Benjamin J. Metcalf, W. Steven Kolthammer, and Ian A. Walmsley. An optimal design for universal multiport interferometers, 2017.
- [4] Michael Conrad. Molecular computing. In *Advances in Computers*, volume 31, pages 235–324. Elsevier, 1990.
- [5] Nathalie P De Leon, Kohei M Itoh, Dohun Kim, Karan K Mehta, Tracy E Northup, Hanhee Paik, BS Palmer, Nitin Samarth, Sorawis Sangtawesin, and David W Steuerman. Materials

Operation	Count in Bidiag	Count in QR-Iter
Addition	$5mn - 10n + 5$	$(18n - 16)C$
Multiplication	$4mn - 8n + 4$	$(28n - 27)C$
Division	$3nm - 6n + 3$	$(4n - 3)C$
Square root	$2nm - 4n + 2$	$(2n - 1)C$
Chip configuration	$2n$	$2C$
Chip operation	$2mn + 2n^2$	$(m + n)C$

Table 9: Operation counts for GRK-SVD (H).

Operation	actual GPU count in Bidiag	actual GPU count in QR-Iter
Addition	$m^3n + 2m^2n - \frac{1}{3}mn^3 - mn^2 + \frac{10}{3}mn - m + \frac{2}{3}n^4 - \frac{1}{3}n^3 - \frac{2}{3}n^2 - \frac{2}{3}n - 3$	$(2n - 2)mC + (2n^2 + 10n - 16)C$
Multiplication	$m^3n + 3m^2n - \frac{1}{3}mn^3 - 2mn^2 + \frac{7}{3}mn - m + \frac{2}{3}n^4 + \frac{1}{3}n^3 - \frac{5}{3}n^2 - \frac{2}{3}n - 2$	$(4n - 4)mC + (4n^2 + 20n - 32)C$

Table 10: Actually by the GPU performed operations for GRK-SVD (D-MC).

challenges and opportunities for quantum computing hardware. *Science*, 372(6539):eabb2823, 2021.

- [6] Zlatko Drmač and Krešimir Veselić. New fast and accurate jacobi svd algorithm. i. *SIAM Journal on matrix analysis and applications*, 29(4):1322–1342, 2008.
- [7] Zlatko Drmač and Krešimir Veselić. New fast and accurate jacobi svd algorithm. ii. *SIAM Journal on matrix analysis and applications*, 29(4):1343–1362, 2008.
- [8] Agner Fog. Instruction tables. *Technical University of Denmark*, 2018.
- [9] George E Forsythe and Richard A Leibler. Matrix inversion by a monte carlo method. *Mathematics of Computation*, 4(31):127–129, 1950.
- [10] George Elmer Forsythe and Peter Henrici. The cyclic jacobi method for computing the principal values of a complex matrix. *Transactions of the American Mathematical Society*, 94(1):1–23, 1960.
- [11] John GF Francis. The qr transformation a unitary analogue to the lr transformation—part 1. *The Computer Journal*, 4(3):265–271, 1961.
- [12] G. Golub and W. Kahan. Calculating the singular values and pseudo-inverse of a matrix. *Journal of the Society for Industrial and Applied Mathematics Series B Numerical Analysis*, 2(2):205–224, 1965.
- [13] G. H. Golub and C. Reinsch. *Singular Value Decomposition and Least Squares Solutions*, pages 134–151. Springer Berlin Heidelberg, Berlin, Heidelberg, 1971.
- [14] Aram W Harrow, Avinatan Hassidim, and Seth Lloyd. Quantum algorithm for linear systems of equations. *Physical review letters*, 103(15):150502, 2009.

Algorithm 2 : QR-decomposition

Input: $\mathbf{A} = \mathbf{A}^{(0)} \in \mathbb{R}^{m \times n}$

- 1: $\mathbf{Q}^{(0)} = \mathbf{I}_{m \times m}$
- 2: Initialize $k = 1$
- 3: **while** $k \leq \min\{m, n\}$ **do**
- 4: Define $\mathbf{a} = (A_{k,k}^{(k-1)}, A_{k+1,k}^{(k-1)}, \dots, A_{m,k}^{(k-1)})^\top \in \mathbb{R}^{m-k+1}$, i.e., \mathbf{a} is the k -th column of $\mathbf{A}^{(k-1)}$ below the diagonal
- 5: Define the unitary matrix

$$\mathbf{U}^{(k)} = \begin{bmatrix} \mathbf{I}_{(k-1) \times (k-1)} & \mathbf{0} \\ \mathbf{0} & \mathbf{U}_{\mathbf{a}-\|\mathbf{a}\|_2 \mathbf{e}_1} \end{bmatrix},$$

where $\mathbf{U}_{\mathbf{v}} = \mathbf{I}_{(m-k+1) \times (m-k+1)} - \frac{2}{\|\mathbf{v}\|_2^2} \mathbf{v} \mathbf{v}^\top$, for $\mathbf{v} \in \mathbb{R}^d$, and $\mathbf{e}_1 \in \mathbb{R}^{m-k+1}$ denotes the first unit vector.

- 6: $\mathbf{A}^{(k)} = \mathbf{U}^{(k)} \cdot \mathbf{A}^{(k-1)}$
- 7: $\mathbf{Q}^{(k)} = \mathbf{Q}^{(k-1)} \cdot \mathbf{U}^{(k)}$
- 8: $k \leftarrow k + 1$
- 9: **end while**

Output: $\mathbf{R} = \mathbf{A}^{(\min\{m,n\})}$ (upper triangular) and $\mathbf{Q} = \mathbf{Q}^{(\min\{m,n\})}$ (unitary) with $\mathbf{A} = \mathbf{Q} \cdot \mathbf{R}$

- [15] Yipeng Huang, Ning Guo, Mingoo Seok, Yannis Tsividis, and Simha Sethumadhavan. Evaluation of an analog accelerator for linear algebra. *ACM SIGARCH Computer Architecture News*, 44(3):570–582, 2016.
- [16] Carl Gustav Jacob Jacobi. Über ein leichtes verfahren die in der theorie der säcularstörungen vorkommenden gleichungen numerisch aufzulösen*. *Journal für die reine und angewandte Mathematik* 30, 1846.
- [17] Vera N Kublanovskaya. On some algorithms for the solution of the complete eigenvalue problem. *USSR Computational Mathematics and Mathematical Physics*, 1(3):637–657, 1962.
- [18] Bruce J MacLennan. A review of analog computing. *Department of Electrical Engineering & Computer Science, University of Tennessee, Technical Report UT-CS-07-601 (September)*, 2007.
- [19] Ashley Montanaro. Quantum algorithms: an overview. *npj Quantum Information*, 2(1):1–8, 2016.
- [20] John Preskill. Quantum computing in the nisq era and beyond. *Quantum*, 2:79, 2018.
- [21] Michael Reck, Anton Zeilinger, Herbert J Bernstein, and Philip Bertani. Experimental realization of any discrete unitary operator. *Physical review letters*, 73(1):58, 1994.
- [22] Artur Scherer, Benoit Valiron, Siun-Chuon Mau, Scott Alexander, Eric Van den Berg, and Thomas E Chapuran. Concrete resource analysis of the quantum linear-system algorithm used to compute the electromagnetic scattering cross section of a 2d target. *Quantum Information Processing*, 16(3):60, 2017.

Algorithm 3 : Golub-Reinsch-Kahan-Bidiagonalization

Input: $\mathbf{A} \in \mathbb{R}^{m \times n}$ with $m \geq n$

- 1: $\mathbf{B}^{(0)} = \mathbf{A}$
- 2: $\mathbf{P}^{(0)} = \mathbf{I}_{m \times m}$
- 3: $\mathbf{Q}^{(0)} = \mathbf{I}_{n \times n}$
- 4: Initialize $k = 1$
- 5: **while** $k \leq n$ **do**
- 6: Define $\mathbf{a} = (\mathbf{B}_{k,k}^{(k-1)}, \mathbf{B}_{k+1,k}^{(k-1)}, \dots, \mathbf{B}_{m,k}^{(k-1)})^\top \in \mathbb{R}^{m-k+1}$, i.e., \mathbf{a} is the k -th column of $\mathbf{B}^{(k-1)}$ below the diagonal, and the unitary matrix

$$\mathbf{U}^{(k)} = \begin{bmatrix} \mathbf{I}^{(k-1) \times (k-1)} & \mathbf{0} \\ \mathbf{0} & \mathbf{U}_{\mathbf{a}-\|\mathbf{a}\|_2 \mathbf{e}_1} \end{bmatrix},$$

where $\mathbf{U}_{\mathbf{v}} = \mathbf{I}_{(m-k+1) \times (m-k+1)} - \frac{2}{\|\mathbf{v}\|_2^2} \mathbf{v} \mathbf{v}^\top$, for $\mathbf{v} \in \mathbb{R}^d$, and $\mathbf{e}_1 \in \mathbb{R}^{m-k+1}$ denotes the first unit vector.

- 7: $\tilde{\mathbf{B}}^{(k)} = \mathbf{U}^{(k)} \cdot \mathbf{B}^{(k-1)}$
- 8: $\mathbf{P}^{(k)} = \mathbf{P}^{(k-1)} \cdot \mathbf{U}^{(k)}$
- 9: Define $\mathbf{b} = (B_{k,k+1}^{(k-1)}, B_{k,k+2}^{(k-1)}, \dots, B_{k,n}^{(k-1)})^\top \in \mathbb{R}^{n-k}$, i.e., \mathbf{b} is the k -th row of $\mathbf{B}^{(k-1)}$ to the right of the superdiagonal. If $k = n$, set $\mathbf{V}^{(k)} = \mathbf{I}_{n \times n}$ and skip the calculations. Define the unitary matrix

$$\mathbf{V}^{(k)} = \begin{bmatrix} \mathbf{I}_{k \times k} & \mathbf{0} \\ \mathbf{0} & \mathbf{V}_{\mathbf{b}-\|\mathbf{b}\|_2 \mathbf{e}_1} \end{bmatrix},$$

where $\mathbf{V}_{\mathbf{v}} = \mathbf{I}_{(n-k) \times (n-k)} - \frac{2}{\|\mathbf{v}\|_2^2} \mathbf{v} \mathbf{v}^\top$, for $\mathbf{v} \in \mathbb{R}^{n-k}$, and $\mathbf{e}_1 \in \mathbb{R}^{n-k}$ denotes the first unit vector.

- 10: $\mathbf{B}^{(k)} = \tilde{\mathbf{B}}^{(k)} \cdot \mathbf{V}^{(k)}$
- 11: $\mathbf{Q}^{(k)} = \mathbf{V}^{(k)} \cdot \mathbf{Q}^{(k-1)}$
- 12: $k \leftarrow k + 1$
- 13: **end while**

Output: $\mathbf{B} = \mathbf{B}^{(n)}$ (bidiagonal), $\mathbf{P} = \mathbf{P}^{(n)}$ (unitary) and $\mathbf{Q} = \mathbf{Q}^{(n)}$ (unitary) with $\mathbf{A} = \mathbf{P} \cdot \mathbf{B} \cdot \mathbf{Q}$

- [23] Naresh R Shanbhag, Subhasish Mitra, Gustavode de Veciana, Michael Orshansky, Radu Marculescu, Jaijeet Roychowdhury, Douglas Jones, and Jan M Rabaey. The search for alternative computational paradigms. *IEEE Design & Test of Computers*, 25(4):334–343, 2008.
- [24] Peter W Shor. Polynomial-time algorithms for prime factorization and discrete logarithms on a quantum computer. *SIAM review*, 41(2):303–332, 1999.
- [25] Ewin Tang. A quantum-inspired classical algorithm for recommendation systems. In *Proceedings of the 51st annual ACM SIGACT symposium on theory of computing*, pages 217–228, 2019.
- [26] Ewin Tang. Quantum principal component analysis only achieves an exponential speedup because of its state preparation assumptions. *Physical Review Letters*, 127(6):060503, 2021.

- [27] Thomas N Theis and H-S Philip Wong. The end of moore's law: A new beginning for information technology. *Computing in science & engineering*, 19(2):41–50, 2017.
- [28] Evangelos Vasilakis. An instruction level energy characterization of arm processors. *Foundation of Research and Technology Hellas, Inst. of Computer Science, Tech. Rep. FORTH-ICS/TR-450*, 2015.

Algorithm 4 : GRK-SVD (Golub, Reinsch, Kahan)

Input: $\mathbf{A} \in \mathbb{R}^{m \times n}$ with $m \geq n$

- 1: Decompose $\mathbf{A} = \mathbf{P} \cdot \mathbf{B} \cdot \mathbf{Q}$ via Algorithm 3
- 2: Set $\mathbf{U}^{(0)} = \mathbf{P}$
- 3: Set $\mathbf{V}^{(0)} = \mathbf{Q}$
- 4: Set $\delta = \varepsilon_0 \|\mathbf{B}\|_\infty$ where ε_0 denotes machine precision
- 5: **while** $\|\mathbf{B} - \text{diag}(\mathbf{B})\|_\infty > \delta$ **do**
- 6: Set the Wilkinson Shift s as the dominant eigenvalue of the bottom right 2x2 minor of $\mathbf{B}^T \mathbf{B}$:

$$s = \max(\sigma(\mathbf{M})), \quad \text{for } \mathbf{M} = \begin{bmatrix} (\mathbf{B}_{n-2,n-1})^2 + (\mathbf{B}_{n-1,n-1})^2 & \mathbf{B}_{n-1,n-1} \mathbf{B}_{n-1,n} \\ \mathbf{B}_{n-1,n-1} \mathbf{B}_{n-1,n} & (\mathbf{B}_{n-1,n})^2 + (\mathbf{B}_{n,n})^2 \end{bmatrix},$$

- 7: Set the desired ratio r_1 of the first two entries in the first column of $\mathbf{B}^T \mathbf{B} - s \mathbf{I}_{n \times n}$ to

$$r_1 = \frac{\mathbf{B}_{1,2} \mathbf{B}_{1,1}}{(\mathbf{B}_{1,1})^2 - s}$$

- 8: Construct the first Givens-Rotation $\mathbf{R}^{(1)}$ as $\mathbf{R}^{(1)} = \widehat{\mathbf{G}}_{1,n}(r_1)$
- 9: Set $\widetilde{\mathbf{D}}^{(1)} = \mathbf{B} \cdot \mathbf{R}^{(1)}$
- 10: $\mathbf{V}^{(1)} \leftarrow (\mathbf{R}^{(1)})^\top \cdot \mathbf{V}^{(0)}$
- 11: Initialize $k = 1$
- 12: **while** $k \leq n - 2$ **do**
- 13: Set $l_k = -\frac{\widetilde{\mathbf{D}}_{k+1,k}^{(k)}}{\widetilde{\mathbf{D}}_{k,k}^{(k)}}$
- 14: Construct Givens-Rotation $\mathbf{L}^{(k)}$ as $\mathbf{L}^{(k)} = \widehat{\mathbf{G}}_{k,m}(l_k)$
- 15: $\mathbf{D}^{(k)} \leftarrow \mathbf{L}^{(k)} \cdot \widetilde{\mathbf{D}}^{(k)}$
- 16: $\mathbf{U}^{(k)} \leftarrow \mathbf{U}^{(k-1)} \cdot (\mathbf{L}^{(k)})^\top$
- 17: Set $r_{k+1} = \frac{\mathbf{D}_{k,k+2}^{(k)}}{\mathbf{D}_{k,k+1}^{(k)}}$
- 18: Construct Givens-Rotation $\mathbf{R}^{(k+1)}$ as $\mathbf{R}^{(k+1)} = \widehat{\mathbf{G}}_{k+1,n}(r_{k+1})$
- 19: $\widetilde{\mathbf{D}}^{(k+1)} \leftarrow \mathbf{D}^{(k)} \cdot \mathbf{R}^{(k+1)}$
- 20: $\mathbf{V}^{(k)} \leftarrow (\mathbf{R}^{(k+1)})^\top \cdot \mathbf{V}^{(k-1)}$
- 21: $k \leftarrow k+1$
- 22: **end while**
- 23: Set $l_{n-1} = -\frac{\mathbf{B}_{n,n-1}}{\mathbf{B}_{n-1,n-1}}$
- 24: Construct the last Givens-Rotation $\mathbf{L}^{(n-1)}$ as $\mathbf{L}^{(n-1)} = \widehat{\mathbf{G}}_{n-1,m}(l_{n-1})$
- 25: $\mathbf{D}^{(n-1)} \leftarrow \mathbf{L}^{(n-1)} \cdot \widetilde{\mathbf{D}}^{(n-1)}$
- 26: $\mathbf{U}^{(n-1)} \leftarrow \mathbf{U}^{(n-1)} \cdot (\mathbf{L}^{(n-1)})^\top$
- 27: $\mathbf{B} \leftarrow \mathbf{D}^{(n-1)}$
- 28: **if** a diagonal element of \mathbf{B} is zero **then**
- 29: Use rotation step (cf. [13] section 1.4 for details)
- 30: **end if**
- 31: **if** a super diagonal element of \mathbf{B} is zero **then**
- 32: Proceed independently with two separate sub-matrices
- 33: **end if**
- 34: **end while**

Output: $\Sigma = \mathbf{B}$ (diagonal), $\mathbf{U} = \mathbf{Q}$ (unitary) and $\mathbf{V} = \mathbf{P}^T$ (unitary) with $\mathbf{A} = \mathbf{U} \cdot \Sigma \cdot \mathbf{V}^T$

Algorithm 5 : Photonics optimized QR-Decomposition

Input: $\mathbf{A} \in \mathbb{R}^{n \times n}$ with $m \geq n$

- 1: $\mathbf{A}^{(0)} = \mathbf{A}$
- 2: $\mathbf{Q}^{(0)} = \mathbf{I}_{m \times m}$
- 3: Initialize $k = 1$
- 4: **while** $k \leq n$ **do**
- 5: Reset Chip
- 6: Initialize $l = m$
- 7: Initialize $d = \mathbf{A}_{m,k}^{(k-1)}$
- 8: **while** $l > k$ **do**
- 9: Compute $r_{k,l} = -\frac{d}{\mathbf{A}_{l-1,k}^{(k-1)}}$
- 10: Program OC to encode $\widehat{\mathbf{G}}_{l-1,l}^n(r_{k,l})$ at $1, l-1$, cf. Figure 3a
- 11: Set $d = \frac{\mathbf{A}_{l-1,k}^{(k-1)} - r_{k,l}d}{\sqrt{1+r_{k,l}^2}}$
- 12: $l \leftarrow l - 1$
- 13: **end while**
- 14: Calculate $\mathbf{A}^{(k)}$ by passing $\mathbf{A}^{(k-1)}$ column-wise through OC
- 15: Calculate $(\mathbf{Q}^{(k)})^T$ by passing $(\mathbf{Q}^{(k-1)})^T$ column-wise through OC
- 16: **end while**

Output: $\mathbf{R} = \mathbf{A}^{(n)}$ (upper triangular) and $\mathbf{Q} = \mathbf{Q}^{(n)}$ (unitary) with $\mathbf{A} = \mathbf{Q} \cdot \mathbf{R}$

Algorithm 6 : Photonics optimized GRK Bidiagonalization

Input: $\mathbf{A} \in \mathbb{R}^{n \times n}$ with $m \geq n$

```

1:  $\mathbf{B}^{(0)} = \mathbf{A}$ 
2:  $\mathbf{P}^{(0)} = \mathbf{I}_{m \times m}$ 
3:  $\mathbf{Q}^{(0)} = \mathbf{I}_{n \times n}$ 
4: Initialize  $k = 1$ 
5: while  $k \leq n$  do
6:   Reset Chip
7:   Initialize  $l = m$ 
8:   Initialize  $d = \mathbf{B}_{m,k}^{(k-1)}$ 
9:   while  $l > k$  do
10:    Compute  $r_{k,l} = -\frac{d}{\mathbf{B}_{l-1,k}^{(k-1)}}$ 
11:    Program OC to encode  $\widehat{\mathbf{G}}_{l-1,l}^m(r_{k,l})$  at  $1, l-1$ , cf. Figure 3a
12:    Set  $d = \frac{\mathbf{B}_{l-1,k}^{(k-1)} - r_{k,l}d}{\sqrt{1+r_{k,l}^2}}$ 
13:     $l \leftarrow l-1$ 
14:  end while
15:  Calculate  $\widetilde{\mathbf{B}}^{(k)}$  by passing  $\mathbf{B}^{(k-1)}$  column-wise through OC
16:  Calculate  $(\mathbf{P}^{(k)})^T$  by passing  $(\mathbf{P}^{(k-1)})^\top$  column-wise through OC
17:  Reset chip
18:  Initialize  $l = n$ 
19:  Set  $d = \mathbf{B}_{k,n}^{(k-1)}$ 
20:  while  $l > k+1$  do
21:    Compute  $s_{k,l} = \frac{d}{\mathbf{B}_{k,l-1}^{(k-1)}}$ 
22:    Program OC to encode  $\widehat{\mathbf{G}}_{l-1,l}^n(s_{k,l})$  at  $1, l-1$ 
23:    Set  $d = \frac{\mathbf{B}_{k,l-1}^{(k-1)} - s_{k,l}d}{\sqrt{1+s_{k,l}^2}}$ 
24:     $l \leftarrow l-1$ 
25:  end while
26:  Calculate  $(\mathbf{B}^{(k)})^\top$  by passing  $(\widetilde{\mathbf{B}}^{(k)})^\top$  column-wise through OC
27:  Calculate  $\mathbf{Q}^{(k)}$  by passing  $\mathbf{Q}^{(k-1)}$  column-wise through OC
28:   $k \leftarrow k+1$ 
29: end while

```

Output: $\mathbf{B} = \mathbf{B}^{(n)}$ (bidiagonal), $\mathbf{Q} = \mathbf{Q}^{(n)}$ (unitary) and $\mathbf{P} = \mathbf{P}^{(n)}$ (unitary) with $\mathbf{A} = \mathbf{P} \cdot \mathbf{B} \cdot \mathbf{Q}$

Algorithm 7 : Photonics optimized GRK-SVD (GRK-SVD H)

Input: $\mathbf{A} \in \mathbb{R}^{m \times n}$ with $m \geq n$. (Note that this Algorithm needs the Chip in a flipped configuration, such that the first two input channels interact first.)

- 1: Decompose $\mathbf{A} = \mathbf{Q} \cdot \mathbf{B} \cdot \mathbf{P}$ via Algorithm 6
- 2: Set $\delta = \varepsilon_0 \|\mathbf{B}\|_\infty$ where ε_0 is the machine precision
- 3: **while** $\|\mathbf{B} - \text{diag}(\mathbf{B})\|_\infty > \delta$ **do**
- 4: Set the Wilkinson Shift s as the dominant eigenvalue of the bottom right 2x2 minor of $\mathbf{B}^T \mathbf{B}$:

$$s = \max(\sigma(\mathbf{M})), \quad \text{for } \mathbf{M} = \begin{bmatrix} \mathbf{B}_{n-2,n-1}^2 + \mathbf{B}_{n-1,n-1}^2 & \mathbf{B}_{n-1,n-1} \mathbf{B}_{n-1,n} \\ \mathbf{B}_{n-1,n-1} \mathbf{B}_{n-1,n} & \mathbf{B}_{n-1,n}^2 + \mathbf{B}_{n,n}^2 \end{bmatrix},$$

- 5: Set the desired ratio r_1 of the first two entries in the first column of $\mathbf{B}^T \mathbf{B} - s \mathbf{I}_{n \times n}$ to

$$r_1 = \frac{\mathbf{B}_{1,2} \mathbf{B}_{1,1}}{\mathbf{B}_{1,1}^2 - s}$$

- 6: Construct the first Givens-Rotation $\mathbf{R}^{(1)}$ as $\mathbf{R}^{(1)} = \widehat{\mathbf{G}}_{1,n}(r_1)$
- 7: Set $\widetilde{\mathbf{D}}^{(1)} = \mathbf{B} \cdot \mathbf{R}^{(1)}$
- 8: Initialize $k = 1$
- 9: **while** $k \leq n - 2$ **do**
- 10: Set $l_k = -\frac{\widetilde{\mathbf{D}}_{k+1,k}^{(k)}}{\widetilde{\mathbf{D}}_{k,k}^{(k)}}$
- 11: Construct Givens-Rotation $\mathbf{L}^{(k)}$ as $\mathbf{L}^{(k)} = \widehat{\mathbf{G}}_{k,m}(l_k)$
- 12: $\mathbf{D}^{(k)} \leftarrow \mathbf{L}^{(k)} \cdot \widetilde{\mathbf{D}}^{(k)}$
- 13: Set $r_{k+1} = \frac{\mathbf{D}_{k,k+2}^{(k)}}{\mathbf{D}_{k,k+1}^{(k)}}$
- 14: Construct Givens-Rotation $\mathbf{R}^{(k+1)}$ as $\mathbf{R}^{(k+1)} = \widehat{\mathbf{G}}_{k+1,n}(r_{k+1})$
- 15: $\widetilde{\mathbf{D}}^{(k+1)} \leftarrow \mathbf{D}^{(k)} \cdot \mathbf{R}^{(k+1)}$
- 16: $k \leftarrow k+1$
- 17: **end while**
- 18: Set $l_{n-1} = -\frac{\mathbf{B}_{n,n-1}}{\mathbf{B}_{n-1,n-1}}$
- 19: Construct the last Givens-Rotation $\mathbf{L}^{(n-1)}$ as $\mathbf{L}^{(n-1)} = \widehat{\mathbf{G}}_{n-1,m}(l_{n-1})$
- 20: $\mathbf{D}^{(n-1)} \leftarrow \mathbf{L}^{(n-1)} \cdot \widetilde{\mathbf{D}}^{(n-1)}$
- 21: Encode all inverses of the matrices $\mathbf{R}^{(k)}$ on the chip, where $(\mathbf{R}^{(k)})^T$ is put at $1, k$
- 22: Calculate $\widetilde{\mathbf{P}}$ by passing \mathbf{P} column-wise through OC which is now configured as in Figure 3b
- 23: Encode all inverses of the matrices $\mathbf{L}^{(k)}$ on the chip, where $(\mathbf{L}^{(k)})^T$ is put at $1, k$
- 24: Calculate $\widetilde{\mathbf{Q}}^T$ by passing \mathbf{Q}^T column-wise through OC, cf. Figure 3b
- 25: $\mathbf{P}, \mathbf{Q} \leftarrow \widetilde{\mathbf{P}}, \widetilde{\mathbf{Q}}$
- 26: $\mathbf{B} \leftarrow \mathbf{D}^{(n-1)}$
- 27: **if** a diagonal element of \mathbf{B} is zero **then**
- 28: Use rotation step (cf. [13] section 1.4 for details)
- 29: **end if**
- 30: **if** a super diagonal element of \mathbf{B} is zero **then**
- 31: Proceed independently with two separate sub-matrices
- 32: **end if**
- 33: **end while**

Output: $\Sigma = \mathbf{B}$ (diagonal), $\mathbf{U} = \mathbf{Q}$ (unitary) and $\mathbf{V} = \mathbf{P}^T$ (unitary) with $\mathbf{A} = \mathbf{U} \cdot \Sigma \cdot \mathbf{V}^T$
